Proceedings of the Seventh International Conference on
Railway Technology: Research, Development and Maintenance
Edited by: J. Pombo
Civil-Comp Conferences, Volume 15, Paper 5.12
Civil-Comp Press, Edinburgh, United Kingdom, 2026
ISSN: 2753-3239, doi: 10.4203/ccc.15.5.12

Optimization of the Cross-Sectional Shape of the Train Body Considering the Influence of Crosswind on High-Speed Trains

G. Zheng and Y. Yu

**Institute of Mechanics, Chinese Academy of Sciences,
Beijing, China**

Abstract

With the continuous increase in the speed of high-speed trains, the comfort, stability and safety of high-speed trains have gradually become the focus of attention. Crosswind has an impact on the safety and comfort of high-speed train operation, and it is a research object that needs to be given priority. This paper considers the influence of crosswind on high-speed trains and uses the research method of simulation analysis to numerically simulate the aerodynamic performance of the cross-sectional shape of the high-speed train body. By comparing and analyzing the force conditions of different geometric shapes of the high-speed train body cross-section under crosswind, the optimal cross-sectional shape of the high-speed train body is obtained, providing a basis for the further development of the shape design of high-speed trains.

Keywords: high-speed train, cross-section, crosswind, numerical simulation, geometric shape, optimization.

1 Introduction

High-speed trains, as one of the most modern means of transportation, can generally reach a maximum speed of over 250 km/h. They not only meet the travel needs of people's daily lives but also provide an indispensable transportation mode for the rapid development of the national economy. With the continuous increase in the speed of high-speed trains, the comfort, stability, and safety of high-speed trains have gradually become the focus of attention.

Since the development of high-speed trains in China in 2003, researchers have never stopped their studies on the aerodynamics of high-speed trains. The numerical simulation calculation methods mainly include finite difference method, finite element method, and boundary element method, etc. [1]. The focus of attention includes air resistance, air pressure pulses, and overturning moments generated by lateral wind forces, etc. [2-3].

Among the many aerodynamic problems of high-speed trains, crosswind has an impact on the safety and comfort of high-speed train operation, and it is a research object that needs to be focused on. In recent years, due to crosswind, there have been numerous high-speed train operation accidents both at home and abroad. For example, in Xinjiang, China, there have been 13 times that trains were blown over by strong winds, and a total of 79 trains overturned. In the Lanzhou-Xinjiang Railway, since its opening, there have been nearly 40 cases of train derailment and overturning caused by strong winds, and blowing over freight cars 110 times. The losses caused by delays and suspensions due to strong winds are incalculable, posing a serious threat to people's lives and property [4].

To improve the safety of train operation in crosswind conditions, researchers at home and abroad have conducted a large number of studies in recent decades. The research results show that the shape of the high-speed train body under crosswind will have a significant impact on the aerodynamic performance it experiences. Due to the long length of the train and the large proportion of the body's cross-sectional part, the lateral aerodynamic effect contributed by the body becomes one of the main factors affecting the lateral stability of the train. By changing the cross-sectional shape of the body, optimizing the lateral force and lift it receives to reduce the overturning moment and lower the risk of train overturning, it is a feasible and effective method [5].

The development of traditional methods for optimizing the cross-sectional shape of high-speed train bodies has been relatively mature, and related technologies have reached a bottleneck period. In recent years, with the rapid development of bionics, the unique structures on the surface of biological organisms provide an inexhaustible source for solving many complex engineering problems.

Summarizing the literature [6-33], we find that non-smooth surfaces in the field of bionics have a significant effect on drag reduction in various fields. In the aerodynamic research of high-speed trains and automobiles, the results show that the body surface with a recessed structure has a better drag reduction effect. Therefore, in order to improve the operating performance of high-speed trains, achieve the trend of lightweight development, increase the safety and comfort of high-speed train operation, and ensure the stability of high-speed train operation, this paper will conduct non-smooth geometric optimization of the cross-sectional shape of the train body considering the influence of crosswind, using the research method of simulation analysis, by comparing and analyzing the force conditions of different geometric shapes of high-speed train body cross-sections under crosswind, to obtain the optimal geometric shape.

2 Research Methods

This study employed simulation analysis methods, as follows:
(1) Utilize the CATIA software to create a geometric model of the cross-section of a high-speed train;
(2) Use software such as ICEM to divide the fluid simulation calculation grid for the cross-section of the high-speed train geometric model;
(3) Employ ANSYS Fluent to conduct fluid simulation calculations for different operating conditions of the high-speed train cross-section;
(4) Utilize software such as Tecplot to process the simulation calculation data and obtain the required data curves and cloud charts.

3 Simulation Results

3.1 Operating Conditions Description

The main purpose of this study is to compare the force conditions of the cross-sectional shapes of high-speed train car bodies under crosswind velocity, and to optimize the cross-sectional shapes of high-speed train car bodies. The crosswind velocity selected is 30 m/s, and the gas state is ideal gas.

3.2 Geometric Model

In order to compare the force conditions of the cross-sectional shapes of high-speed train car bodies with different geometric forms under crosswind velocity, this paper will select five geometric forms, as shown in Figure 1.

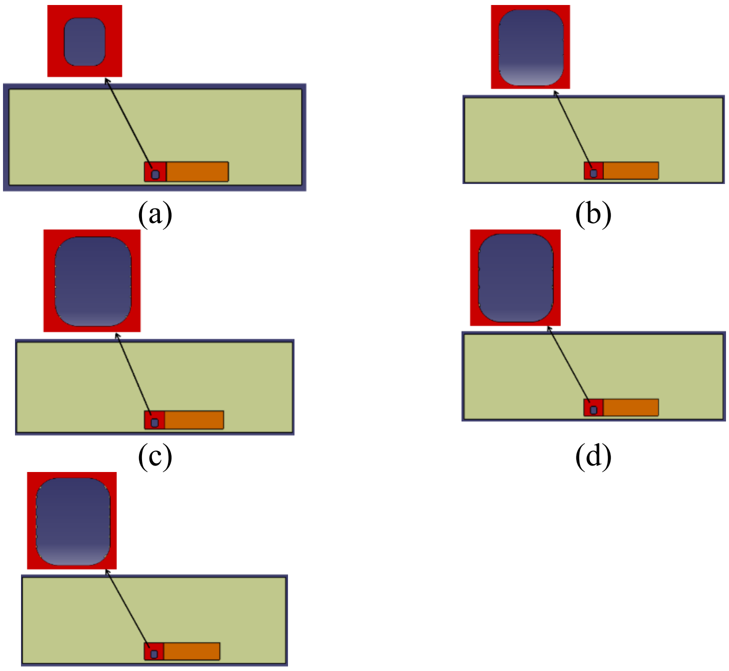
(a) (b) (c) (d) (e)

Figure 1: Geometric Model of High-Speed Train Car Body Cross-Section.

Among them, the geometric shape shown in Figure 1(a) is the unoptimized cross-sectional shape of the high-speed train car body, with a cross-sectional width of 3400mm, a height of 4000mm, and a height from the ground of 2800mm. To facilitate the subsequent aerodynamic grid division, during the establishment of the cross-sectional shape geometric model of the high-speed train car body, the far-field model was also established. In the far-field, we set the width to 136000mm and the height to 44800mm.

Based on the unoptimized cross-sectional shape geometric form of the high-speed train car body, we used depressions on the cross-sectional surface as a means to optimize the geometric form. The shapes were selected as circular and elliptical.

Figure 1(b) and Figure 1(c) show the geometric forms with circular depressions on the original cross-sectional shape of the high-speed train car body, with the radius size of the circular depressions being 50mm, and the area proportions selected as 10% and 20% respectively.

Figure 1(d) and Figure 1(e) show the geometric forms with elliptical depressions on the original cross-sectional shape of the high-speed train car body, with the dimensions of the elliptical depressions being 100mm for the long axis and 50mm for the short axis, and the area proportions selected as 10% and 20% respectively.

3.3 Grid Division

After the geometric model of the cross-section of the high-speed train body is established, we need to perform aerodynamic grid division using ICEM, obtaining the aerodynamic grids as shown in Figure 2.

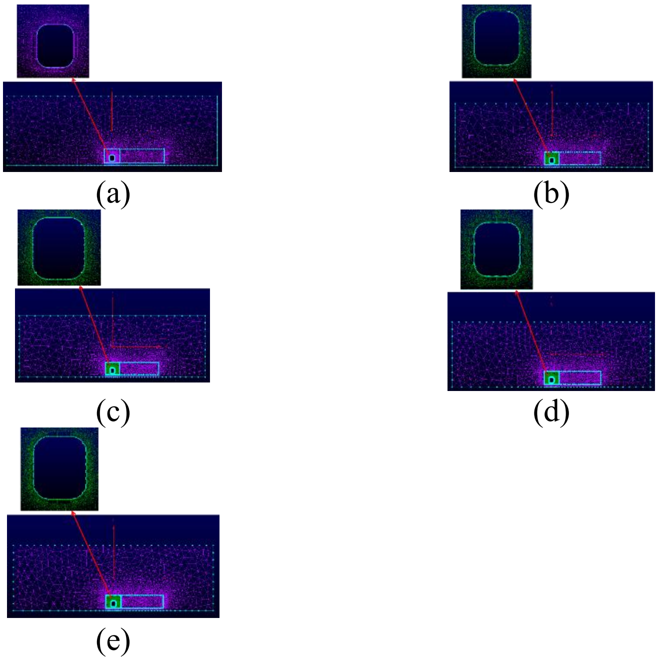

Figure 2: Cross-sectional grid model of the high-speed train body.

Figure 2(a) corresponds to the original unoptimized cross-sectional view of the high-speed train body, with a non-structured grid form. The height of the first layer of the boundary layer is set to 0.001mm, the growth rate is set to 1.3, the boundary layer grid uses quadrilaterals, and the growth is 50 layers, with a total of 12,110 grids.

Figure 2(b) corresponds to the cross-sectional view of the high-speed train body with 10% area circular depressions, with the same non-structured grid form. The height of the first layer of the boundary layer is set to 0.001mm, the growth rate is set to 1.3, the boundary layer grid uses quadrilaterals, and the growth is 50 layers, with a total of 13,543 grids.

Figure 2(c) corresponds to the cross-sectional view of the high-speed train body with 20% area circular depressions, with the same grid settings as the cross-sectional view with 10% area circular depressions. The total number of grids is 18,654.

Figure 2(d) corresponds to the cross-sectional view of the high-speed train body with 10% area elliptical depressions, with a non-structured grid form. The height of the first layer of the boundary layer is set to 0.001mm, the growth rate is set to 1.3, the boundary layer grid uses quadrilaterals, and the growth is 50 layers, with a total of 13,987 grids.

Figure 2(e) corresponds to the cross-sectional view of the high-speed train body with 20% area elliptical depressions, with the same non-structured grid form. The height of the first layer of the boundary layer is set to 0.001mm, the growth rate is set to 1.3, the boundary layer grid uses quadrilaterals, and the growth is 50 layers, with a total of 20,213 grids.

3.4 Numerical Simulation Calculation

3.4.1 Numerical Simulation Calculation Settings

Before selecting the solver, it is necessary to check the imported mesh to ensure that the minimum volume value is positive. Then, the mesh size units need to be unified. The problem studied in this paper belongs to subsonic incompressible flow, so we choose a pressure-based solver, and the discretization method is the finite volume method. The turbulence model selected in this paper is the two-equation model, and the energy equation needs to be enabled. The fluid material is selected as ideal gas, and the viscosity calculation uses the Sutherland three-coefficient method.

Boundary condition settings are as follows:

(1) Reference pressure is set to 101325 Pa

(2) Speed inlet boundary condition settings

The inlet boundary condition is set as a speed inlet. The cross-section of the high-speed train body under study is the cross-section of the train body, and the air inflow direction is in the positive X direction. Therefore, we set X-Component of Flow Direction as 1 and Y-Component of Flow Direction as 0.

(3) Pressure outlet boundary condition settings

The outlet boundary condition is set as a pressure outlet, and the boundary-parallel method is selected for the recirculation identification.

(4) Far-field boundary condition settings

The far-field boundary condition is set as a pressure far-field boundary condition. The Mach number is set to 0.088. It should be noted that the X-Component of Flow Direction and Y-Component of Flow Direction here need to be consistent with the settings in the speed inlet boundary condition.

(5) Wall boundary condition settings

The wall is set as a no-slip boundary condition, that is, we assume that the velocity of the fluid at the wall is zero.

Since the cross-section of the high-speed train body under study is a two-dimensional problem, regarding the characteristic values of this numerical simulation, we set the characteristic length to 1m and the characteristic area to 4m2, which is consistent with the cross-sectional height.

The solving method we choose is the coupled solving algorithm, and the grid gradient discretization method we choose is the Green-Gauss Cell Based method. Except for Turbulent Kinetic Energy and Turbulent Dissipation Rate, the difference schemes of the other equations all use the second-order upwind scheme.

Regarding the solving control parameters, the Courant number is set to 200, and the relaxation factor is kept at the default value. The initialization is selected as the default Hybrid Initialization method, and the initial domain is selected as the inlet.

3.4.2 Numerical Simulation Calculation Results

Through the above numerical simulation parameter settings, numerical simulation calculations are performed for several different cross-sectional models of high-speed train bodies, and the following results are obtained, including the drag-time curve, lift-time curve, and overturning moment-time curve. We will compare and analyze the calculation results below.

(1) Comparison of high-speed train body cross-section with circular depression

The numerical simulation data of the high-speed train body cross-section before optimization and the numerical simulation data of the high-speed train body cross-section with circular depressions arranged at 10% of the area are compared. The results are as follows. Figure 3 shows the variation of resistance with time for both cases. From the curve values and trend, it can be seen that as time increases, the resistance value of the cross-section of the high-speed train body with circular depressions arranged at a 10% area ratio is slightly slower in its change compared to the cross-section of the high-speed train body before optimization, and the trend of resistance value change throughout the cycle slows down, with the maximum amplitude decreasing by approximately 143.087N and the minimum value increasing by approximately 145.297N, while the average value increases by approximately 9.514N.

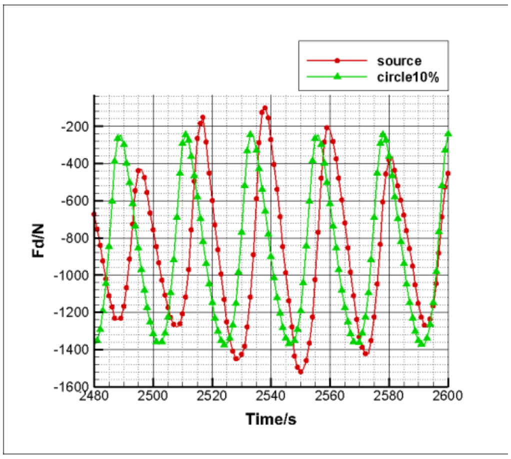

Figure 3: Resistance - Time Curve.

Figure 4 compares the variation of lift with time for both cases. From the curve values and trend, it can be seen that as time increases, the lift value of the cross-section of the high-speed train body with circular depressions arranged at a 10% area ratio is slightly slower in its change compared to the lift value of the cross-section of the high-speed train body before optimization, and the trend of lift value change throughout the cycle slows down, but the maximum amplitude increases by approximately 114.378N, the minimum value increases by approximately 243.112N, and the average value increases by approximately 18.697N.

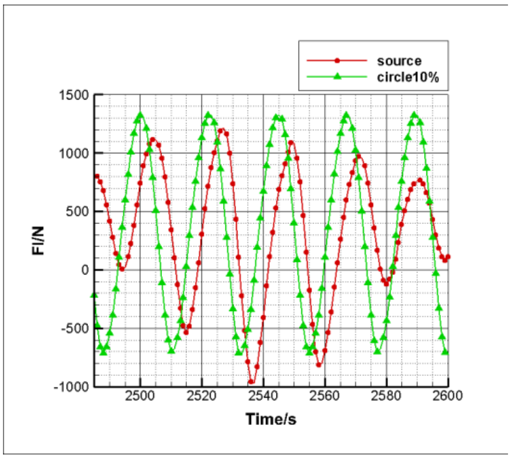

Figure 4: Lift - Time Curve.

Figure 5 compares the variation of overturning moment with time for both cases. From the curve values and trend, it can be seen that as time increases, the overturning moment value of the cross-section of the high-speed train body with circular depressions arranged at a 10% area ratio is slightly slower in its change compared to the overturning moment value of the cross-section of the high-speed train body before optimization, and the trend of overturning moment value change throughout the cycle slows down, with the maximum amplitude decreasing by approximately 25.891N*m, but the minimum value increases by approximately 70.907N*m, and the average value increases by approximately 23.564N*m.

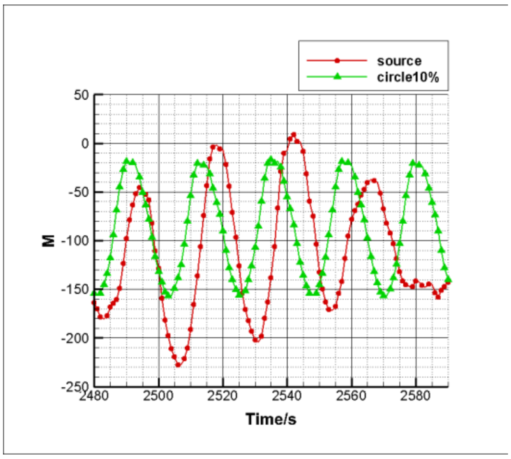

Figure 5: Overturning Moment - Time Curve.

(2) Comparative analysis of the cross-section of the high-speed train body with elliptical depressions

The numerical simulation data of the cross-section of the high-speed train body before optimization and the cross-section of the high-speed train body with elliptical depressions arranged at a 10% area ratio are compared. The results are as follows.

Figure 6 compares the variation of resistance with time for both cases. From the curve values and trend, it can be seen that as time increases, the resistance value of the cross-section of the high-speed train body with elliptical depressions arranged at a 10% area ratio is slightly slower in its change compared to the resistance value of the cross-section of the high-speed train body before optimization, and the trend of resistance value change throughout the cycle slows down, with the maximum amplitude decreasing by approximately 259.719N, and the average value decreasing by approximately 59.823N, but the minimum value increases by approximately 144.113N.

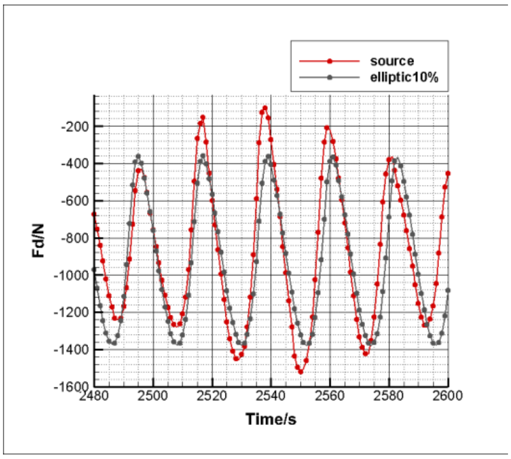

Figure 6: Resistance - Time Curve.

Figure 7 compares the variation of lift with time for both cases. From the curve values and trend, it can be seen that as time increases, the lift value of the cross-section of the high-speed train body with elliptical depressions arranged at a 10% area ratio is slightly slower in its change compared to the lift value of the cross-section of the high-speed train body before optimization, and the trend of lift value change throughout the cycle slows down, but the maximum amplitude decreases by approximately 119.425N, but the minimum value increases by approximately 541.121N, and the average value increases by approximately 72.129N.

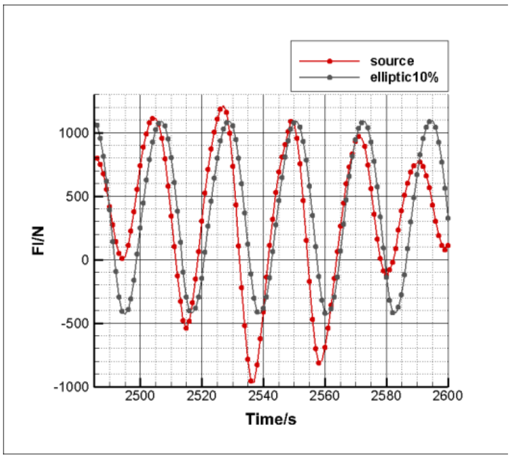

Figure 7: Lift - Time Curve.

Figure 8 compares the variation of overturning moment with time for both cases. From the curve values and trend, it can be seen that as time increases, the overturning moment value of the cross-section of the high-speed train body with elliptical depressions arranged at a 10% area ratio is slightly faster in its change compared to the overturning moment value of the cross-section of the high-speed train body before optimization, and the trend of overturning moment value change throughout the cycle slows down, with the maximum amplitude decreasing by approximately 50.773N*m, but the minimum value increases by approximately 84.497N*m, and the average value increases by approximately 17.125N*m.

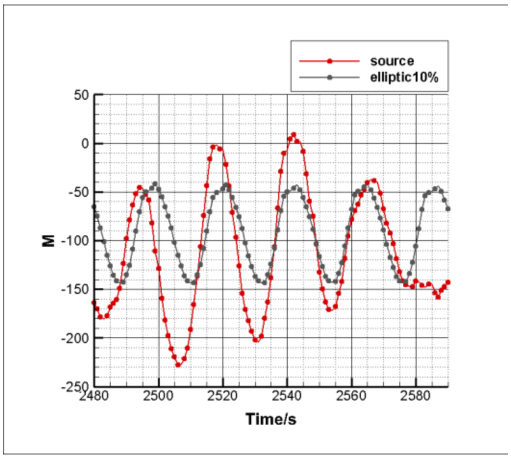

Figure 8: Overturning Moment - Time Curve.

Summarizing the above data results, as shown in the table below, it can be seen that although circular depressions have an advantage over elliptical depressions in reducing the cross-sectional resistance and lift of the high-speed train body, elliptical depressions are more effective in reducing the overturning moment of the cross-sectional area of the high-speed train body. Therefore, this paper finally selects elliptical depressions as the geometric shape for optimizing the cross-sectional area of the high-speed train body.

Data Parameters		10% Circular	10% Elliptical	Comparison Results
Drag Force	Maximum Value	-143.087	-259.719	Circular
	Minimum Value	145.297	-59.823	Circular
	Average Value	9.514	144.113	Elliptical
Lift Force	Maximum Value	114.378	-119.425	Elliptical
	Minimum Value	243.112	541.121	Circular
	Average Value	18.697	72.129	Circular
Listening Moment	Maximum Value	-25.891	-50.773	**Elliptical**
	Minimum Value	70.907	84.497	Circular
	Average Value	23.564	17.125	**Elliptical**

Table 1: Comparison Results of Different Geometric Simulation Data.

(3) Comparative Analysis of Elliptical Pits with Different Proportions

Next, we will conduct a comparative analysis of the numerical simulation results of the cross-sectional profiles of the high-speed train car bodies with elliptical pits at different area proportions, to determine the optimal geometric shape.

As shown in Figure 9, the resistance-time curves of the high-speed train car body cross-sections with elliptical pits arranged at 10% area proportion and those with elliptical pits arranged at 20% area proportion were fitted and analyzed. The results show that the resistance trends of both geometric shapes change relatively smoothly over time. The resistance value of the high-speed train car body cross-section with elliptical pits arranged at 10% area proportion is significantly higher than that of the one arranged at 20% area proportion, but the change speed is slower.

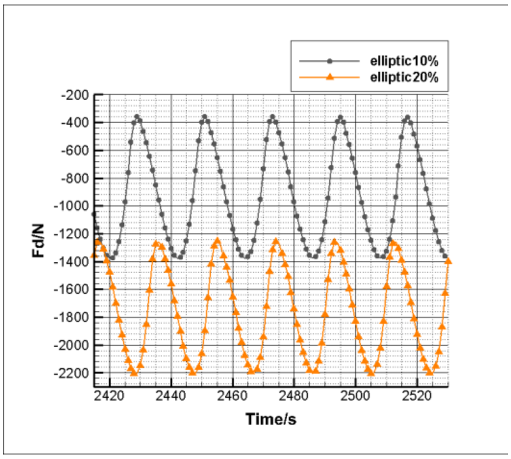

Figure 9: Resistance-time Curve.

Figure 10 is the fitting analysis of the lift-time curves of the high-speed train car body cross-sections with elliptical pits arranged at 10% area proportion and those with elliptical pits arranged at 20% area proportion. The results show that the lift trends of both geometric shapes change relatively smoothly over time. The lift value of the high-speed train car body cross-section with elliptical pits arranged at 10% area proportion is significantly higher than that of the one arranged at 20% area proportion, but the change speed is slower.

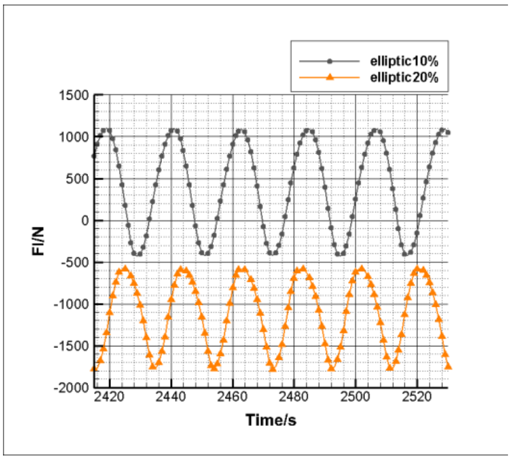

Figure 10: Lift-time Curve.

Figure 11 is the fitting analysis of the overturning moment-time curves of the high-speed train car body cross-sections with elliptical pits arranged at 10% area proportion and those with elliptical pits arranged at 20% area proportion. The results show that the overturning moment trends of both geometric shapes change relatively smoothly over time. The overturning moment value of the high-speed train car body cross-section with elliptical pits arranged at 10% area proportion is significantly higher than that of the one arranged at 20% area proportion, but the change speed is slower.

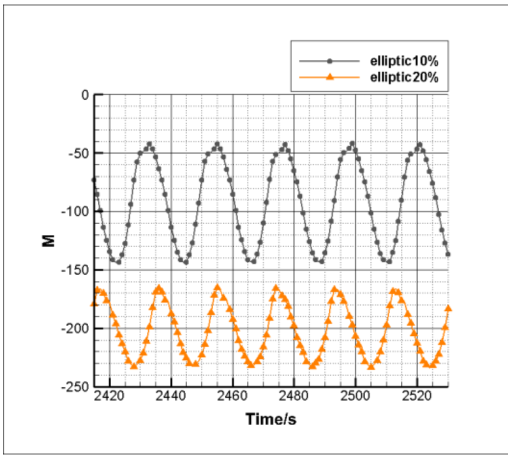

Figure 11: Overturning Moment-time Curve.

4 Conclusions and Contributions

This study employed a simulation analysis method to conduct aerodynamic flow field simulation calculations on the cross-sectional shape of high-speed train bodies under crosswind conditions, and obtained the optimal geometric shape of the high-speed train body cross-section. The conclusions are as follows:

(1) Numerical simulation calculations were performed for different shapes of high-speed train body cross-sections, and the calculated data curves were compared and analyzed. It was concluded that arranging depressions on the surface of the high-speed train body cross-section can effectively reduce the overturning moment of the high-speed train body under crosswind conditions.

(2) Numerical simulations were conducted for high-speed train body cross-sections with different area ratios of elliptical depressions. The simulation results showed that with an area ratio of 20%, the overturning risk of the high-speed train body under crosswind conditions could be significantly reduced.

Therefore, our current research has reached the final optimized geometric shape of the high-speed train body cross-section, which is the high-speed train body cross-section with an elliptical depression having an area ratio of 20%.

References

[1] L.Y. Zhou, J.F. Chen, "Research progress on aerodynamic technology of high-speed trains", Technology and Application, 143.

[2] G.D. Lu, "Aerodynamic problems of high-speed trains", Rolling Stock, 44(10), 1-3, 2006.

[3] Y.R. Chen, Y.G. Xiao, " Calculation of aerodynamic performance of high-speed trains", Rolling Stock, 47(1), 14-16, 2009.

[4] X.B. Li, Z. Yang, J.Y. Zhang, W.H. Zhang, "Aerodynamic performance of high-speed trains in strong crosswinds", Journal of Traffic and Transportation Engineering, 9(2), 66-73, 2009.

[5] J.P. Xiao, Z.X. Huang, L. Chen, "Review of aerodynamic research techniques for high-speed trains", Mechanics and Practice, 35(2), 1-12, 2013.

[6] T.Y. Dong, M. Zhong, X.F. Liang, "Optimization of train cross-sectional shape in windy environments, Journal of the China Railway Society, 42(1), 40-45, 2020.

[7] P. Shen, "Overview of high-speed train aerodynamics research at home and abroad", Science and Technology Innovation Herald, 3(51), 8-9, 2014.

[8] Y.C. Yan, Z. Tang, N. Gao, C. Wang, "Research progress on high-speed train styling design based on aerodynamics", Journal of Machine Design, 34(6), 105-112, 2017.

[9] H.Q. Tian, X.F. Liang, P. Xu, "Research on train aerodynamic performance and methods for shape and structure design", China Railway Science, 23(5), 138-141, 2002.

[10] M.G. Yu, T. Li, Q. Zhang, J.L. Liu, "Aerodynamic performance of high-speed trains under heavy rainfall conditions", Journal of Traffic and Transportation Engineering, 19(5), 96-105, 2019.

[11] Y.C. Chen, "Study on aerodynamic characteristics of high-speed trains under crosswind at tunnel exits", Southwest Jiaotong University, 2021.

[12] H.Q. Tian, "Research progress and development thoughts on aerodynamics of high-speed rail transit in China", Strategic Study of Chinese Academy of Engineering, 17(4), 30-41, 2015.

[13] H.Q. Tian, "Research progress on train aerodynamics in China", Journal of Traffic and Transportation Engineering, 6(1), 1-9, 2006.

[14] H.L. Liu, Z.G. Yang, Y.W. Wu, J.Y. Gao, X.M. Tan, "Simulation study on aeroacoustic performance of high-speed trains at 250–400 km/h", Journal of Railway Science and Engineering, 2022.

[15] X.G. Sheng, M.G. Yu, T. Li, J.L. Liu, "Multi-objective wind-resistant optimization design of high-speed train dynamic parameters", Journal of Machine Design, 40(1), 1-7, 2023.

[16] Z.Q. Li, L.J. Huang, L. Zhou, H. Yang, B.W. Tang, "Sliding mode active disturbance rejection adhesion control method for high-speed trains", Journal of Traffic and Transportation Engineering, 23(2), 251-263, 2023.

[17] D.K. Chen, X.X. Cui, L. Su, X.L. Liu, L.W. Zhang, H.W. Chen, "Current status and progress of drag reduction on fish-like surfaces", China Surface Engineering, 36(5), 14-36, 2023.

[18] D.L. Fan, "Preparation and performance study of non-smooth drag reduction components inspired by pufferfish surface", Jiangsu University of Science and Technology, 2022.
[19] S.Z. Huang, W. Gao, W. Yu, S.J Yu, "Aerodynamic characteristics analysis of non-smooth surface car body", Automotive Engineer, 6, 31-34, 2020.
[20] X.J. Ruan, "Research on improvement of wall flow field simulation method for non-smooth surface car body", Jilin University, 2020.
[21] J.C. Liu, E.Y. Chen, A.L. Yang, G.P. Li, "Study on aerodynamic and noise reduction characteristics of non-smooth surface blades", Thermal Power Engineering, 35(12), 31-39, 2020.
[22] Q. Zhang, J. Song, W.W. Song, S.Q. Yang, Y.X. Zhao, "Study on influence of non-smooth structured impeller on noise reduction of centrifugal pump", China Rural Water and Hydropower, 2023.
[23] J. Tang, Y.Y. Liu, Y.T. Yan, "Drag reduction characteristics of bionic non-smooth surface for underwater vehicles", Acta Armamentarii, 43(5), 1135-1143, 2022.
[24] R.J. Zhang, "Research on aerodynamic drag reduction of MIRA model based on bionic features", Jilin University, 2023.
[25] M. Li, "Numerical study on turbulence enhancement effect and flow control of non-smooth elements", Jilin University, 2020.
[26] L.G. Qin, C.Y. Gong, H.J. Sun, H. Xi, Fagla Jules Mawignon, F.F. Guo, G.N. Dong, "Research progress on drag reduction of non-smooth surfaces", Surface Technology, 51(8), 107-122, 2022.
[27] X. Liu, G.F. Wang, H.J. Cao, "Numerical study on drag reduction technology of dimpled surfaces", Contemporary Chemical Industry, 52(1), 167-171, 2023.
[28] C.T. Kuai, W.Q. Wang, Y.L. Wu, B. Wang, S.N. Du, G.F. Wang, "Numerical simulation study on drag reduction technology of dimpled non-smooth surfaces", Journal of Mechanical Strength, 43(3), 700-706, 2021.
[29] H.F. Yang, "Study on flow around a cylinder with dimpled surface and its drag reduction characteristics", Jiangsu University of Science and Technology, 2021.
[30] C.W. Wang, "Study on influence of non-smooth surface structure on air resistance and friction noise of high-speed electric multiple units", East China Jiaotong University, 2021.
[31] H.T. Hu, "Study on drag reduction characteristics of bionic non-smooth surface and its influence on noise for high-speed trains", East China Jiaotong University, 2020.
[32] H.Y. Zhu, H.T. Hu, B.C. Yin, Z.H. Zhu, C.W. Wang, "Study on drag and noise reduction of high-speed trains with spherical non-smooth surfaces", Noise and Vibration Control, 40(6), 46-51, 2020.
[33] T.E. Hu, D. Zhou, L.L. Wu, Z.X. Cao, "Influence of bionic dimple spacing on aerodynamic drag reduction of high-speed maglev trains", Journal of the China Railway Society, 45(7), 55-61, 2023.